공학석사 학위논문

# Electrochemical Characterization of Prussian Blue Analogues for Aqueous Secondary Batteries

## 수계 이차전지 적용을 위한 프러시안블루 유사체의 전기화학적 특성연구

2020년 2월

서울대학교 대학원
화학생물공학부

김 양 문

# Electrochemical Characterization of Prussian Blue Analogues for Aqueous Secondary Batteries

지도교수 최장욱

이 논문을 공학석사 학위논문으로 제출함
2019년 12월

서울대학교 대학원
화학생물공학부
김 양 문

김 양 문의 공학석사 학위논문을 인준함
2019년 12월

위 원 장 _____ 성 영 은 _____ (인)

부위원장 _____ 최 장 욱 _____ (인)

위 원 _____ 이 규 태 _____ (인)

# Abstract

## Electrochemical Characterization of Prussian Blue Analogues for Aqueous Secondary Batteries

YangMoon Kim
School of Chemical and Biological Engineering
The Graduate School
Seoul National University

Lithium ion batteries (LIBs) have changed our lifestyle and industrial structure with unprecedented high capacity and cyclability. However, because of cost issue related to raw materials and safety issue related to flammable organic electrolyte, new energy storage systems are required. One such system is aqueous battery using water as a solvent of electrolyte. Despite its obvious merits, the lack of electrode materials for this system prevents its commercial use.

Prussian blue analogues (PBAs), a kind of MOF (Metal Organic Framework) are drawing attention as alternative electrode

materials for aqueous battery system due to their unique open framework structure that can accommodate hydrated ion with various ionic radius. Although the synthesis of PBAs is simple and economical, because of its high reaction rate, it is hard to control the structural properties. To investigate a relationship between electrochemical performances and differences in crystal structure derived from the different synthesis methods, PBAs were synthesized through two different methods where one is very fast and the other is very slow. And then, they were electrochemically tested for aqueous sodium ion battery (ASIB) system and aqueous zinc ion battery (AZIB) system, respectively. As a result, in ASIB, slowly synthesized PBA showed higher electrochemical perfor-mance than rapidly synthesized one, on the other hand, in AZIB, the opposite trend appeared. To confirm the cause of this trend, further electrochemical tests for ASIB and AZIB were conducted and it was found that zinc ion and sodium ion have different electrochemical behavior in terms of solid-state diffusion. This series of results suggest that the relationship between electrochemical performances and the structure of PBAs depends on the species of ion which participate in the electrochemical reaction.

Keywords: Prussian blue analogues, aqueous sodium ion battery, aqueous zinc ion battery, electrochemical performance, synthesis

Student Number: 2018-28428

# Table of Contents

# List of Tables

# List of Figures

occurs from cubic phase to rhombohedral phase. (The peak under asterisk belongs to current collector.)

**Figure 10**. Comparison of electrochemical performance between CP-CoHCF and SM-CoHCF. (a) Rate capability profile. Compared to the specific capacity at 1C, that of 5 C was 80% and 10C was 68% for CP-CoHCF, and SM-CoHCF showed 79% and 63%, respectively. (b) Long-term cycle stability profile. CP-CoHCF showed 76% capacity retention over 250 cycles at 5 C, while SM-CoHCF showed only 37%.

**Figure 11**. (a) GCD plot of CuHCF in aqueous zinc ion electrolyte at 1 C-rate(=50 mA/g) in the range of 0.25 V – 1.1 V. (b) Differential capacity analysis profile of CuHCF in aqueous zinc ion electrolyte with different concentration of proton.

**Figure 12**. Rate capability profile of SM-CuHCF and CP-CuHCF. Compared to the specific capacity at 1 C, that of 5 C was 88% and 10 C was 82% for SM-CuHCF and CP-CuHCF showed 67% and 56% respectively.

**Figure 13**. (a) GCD profile of CuHCF in sodium ion aqueous electrolyte at 1 C-rate (=50 mA/g) in the range of 0.25 V – 1 V. (b) Rate capability profile of SM-CuHCF in sodium ion and zinc ion aqueous solution. In sodium ion battery system, compared to the specific capacity at 1 C, that of 5 C was 101% and 10 C was 99%.

**Figure 14**. XANES plot of CuHCF electrode. (a) Copper K-edge peak for sodium ion battery system. (b) Iron K-edge peak for sodium ion battery system. (c) Copper K-edge peak for zinc ion battery system. (d) Iron K-edge peak for zinc ion battery system.

# Chapter 1. Introduction

Since the development of lithium ion intercalation materials which show high energy density and cycle-stability, lithium ion batteries (LIBs) have been applied to many kinds of commercial devices ranging from portable electronic devices such as smartphone to electric vehicles and smart grids[1,2]. The organic solvents (e.g. EC, DEC, DMC, ...) used in LIBs make high operating potential possible, but they also have the limits of high fabrication cost and low safety[3]. Moreover, with massive use of LIBs in the large-scale application such as electric vehicles and energy storage system (ESS), problems like increase of lithium cost and decrease of Li reserves arise[4]. To address these challenges, there has been a lot of efforts to find low-cost and material abundant alternatives to organic LIBs[5].

One of such alternatives is the use of metal ions other than lithium whose reserves are abundant. Candidates for these metal ions are sodium ($Na^+$), potassium ($K^+$), magnesium ($Mg^{2+}$), Calcium ($Ca^{2+}$), zinc ($Zn^{2+}$) and Aluminum ($Al^{3+}$) [6-11]. However, as long as organic solvents are used, the safety and fabrication cost issues cannot be solved. Hence, the use of aqueous electrolytes instead of organic one has been recommended as a promising solution because the water is inexpensive, easy to handle and non-flammable[12]. So, when the aqueous electrolyte is combined with non-lithium

metal ion system, they can be synergic in terms of price and safety, especially for large scale energy storage. However, it is hard to find appropriate electrode material for this aqueous non-lithium metal ion battery system. It is because working potential of active material must be within the range of electrochemical window of water, 1.23 V and ionic radius of non-lithium ions is too large to be sufficiently mobile in a conventional transition metal oxide electrode host [13,14].

Prussian Blue (Iron hexacyanoferrate) and its analogues (PBAs) are a family of transition metal hexacyanometallates whose chemical formula can be expressed as $A_xM_1[M_2(CN)_6]_y*zH2O$ (A denotes an alkali metal ion, $M_1$ and $M_2$ are transition metal ions)[15]. The lattice structure of PBAs consists of octahedral coordination bonds of two kinds of transition metal cations with six cyanide ligands ($CN^-$). The two transition metal ions are connected to each other by cyanide ligands in a way that one makes coordination bond to nitrogen atom and the other to carbon atom (figure 1). In this way, with linear cyanide ligands, PBAs are able to have three-dimensional open framework structure, so that large ionic channels and interstices are possible. In addition, PBAs have advantage of being economical and environmentally friendly because they are synthesized in a simple single coprecipitation reaction in aqueous phase at relatively low temperature. Benefiting from structural and synthetic characteristics, PBAs have been investigated as an eco-friendly and low-cost electrode material for metal ion batteries that have larger ionic radius than lithium[16].

Meanwhile, the structural stability and crystallinity of PBAs depend on synthetic methods because their synthesis is complete rapidly. In this study, to investigate the relationship between structure difference of PBAs and their electrochemical property, I synthesized PBAs with different reaction rate to have different structural characteristics. Cobalt hexacyanoferrate and copper hexacyanoferrate were synthesized each for aqueous sodium and aqueous zinc ion battery system. The reason I choose sodium and zinc among various metal ions is that they each have distinct advantages. First of all, sodium ion is lighter than any other metal ions except lithium ion, so high gravimetric energy density can be realized. On the other hand, although zinc has more than twice the atomic mass than sodium, the fact that zinc metal (−0.76 V vs S.H.E, 820 mAh/g) can be used as anode in aqueous environment makes zinc ion battery attractive[17]. In addition, I choose hexacyano−ferrates ($M_2$=Fe) because they have adequate redox potential to be used as cathode materials for aqueous battery system[18].

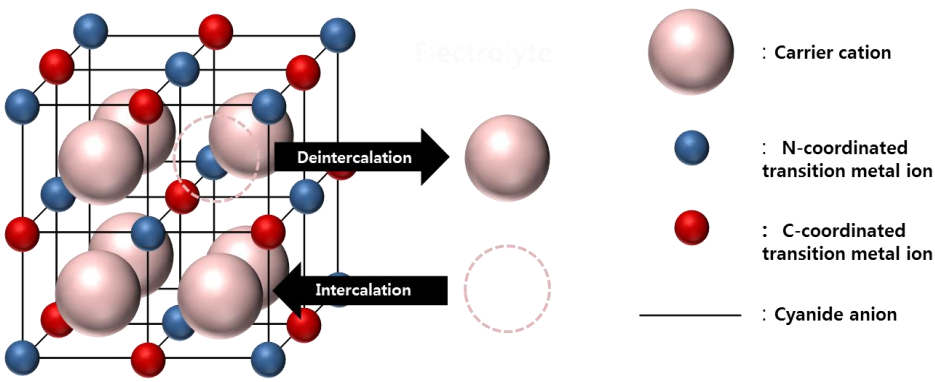


**Figure 1.** Schematic illustration of the general crystal structure and redox reaction of PBAs.

# Chapter 2. Results and Discussion

## 2.1 Synthesis procedure

The synthetic procedure of cobalt hexacyanoferrate (CoHCF) and copper hexacyanoferrate (CuHCF) is schematically illustrated in Figure 2. CoHCF is synthesized using an aqueous solution of cobalt precursor ($Co^{2+}$) and ferrocyanide anion ($[Fe(CN)_6]^{2-}$)precursor, and CuHCF is synthesized using an aqueous solution of copper precursor ($Cu^{2+}$) and ferricyanide anion ($[Fe(CN)_6]^{3-}$)precursor. The reaction proceeds as each transition metal ion forms a coordination bond with the nitrogen atom of cyanide ligand. Meanwhile, the synthesis of PBAs is so fast that the reaction is complete as soon as two precursor solutions are mixed. So, it is difficult to obtain a thermodynamically stable phase, unlike transition metal oxides which are reacted slowly at very high temperatures. To get PBAs with thermodynamically stable phase, the reaction rate should be reduced externally. Herein, I use both physical and chemical methods.

By using peristaltic pump (inner diameter of tube = 1.42 mm), in the way that one end of pump is connected to precursor solution and the other end to deionized water (DI water), two precursor solutions drop into DI water drop by drop. This is a physical method which reduces the amount of reactants reacting per

unit time. However, this method alone has its limitation to get PBAs of stable phase. So, 'Chemical inhibition' method was done with peristaltic pump. Chemical inhibition is the way that reduce reaction rate by using 'Chemical inhibitor' which increases the activation energy of the reaction. I use sodium citrate as chemical inhibitor. Before the reaction of two precursor solutions, sodium citrate is added to the transition metal precursor aqueous solution. The transition metal ion forms a complex with the citrate ion, which lowers the energy of transition metal ion through stabilization. As a result, the activation energy of reactants is raised and because of slow reaction, sufficient time for PBAs to be synthesized in a thermodynamically stable structure is guaranteed[19](Figure 3).

To compare electrochemical performances according to synthesis method of CoHCF as a cathode material for aqueous sodium ion batteries, simply mixed CoHCF (SM-CoHCF) which is synthesized in a way that two precursor solution were poured into DI water at once, and CoHCF using citrate anion and peristaltic pump (CP-CoHCF) were prepared. Also, to compare electro-chemical property according to synthesis method of CuHCF as a cathode material for aqueous zinc ion batteries, SM-CuHCF and CP-CuHCF were synthesized in the same way as already mentioned. Detailed experimental procedure is described in the next chapter.

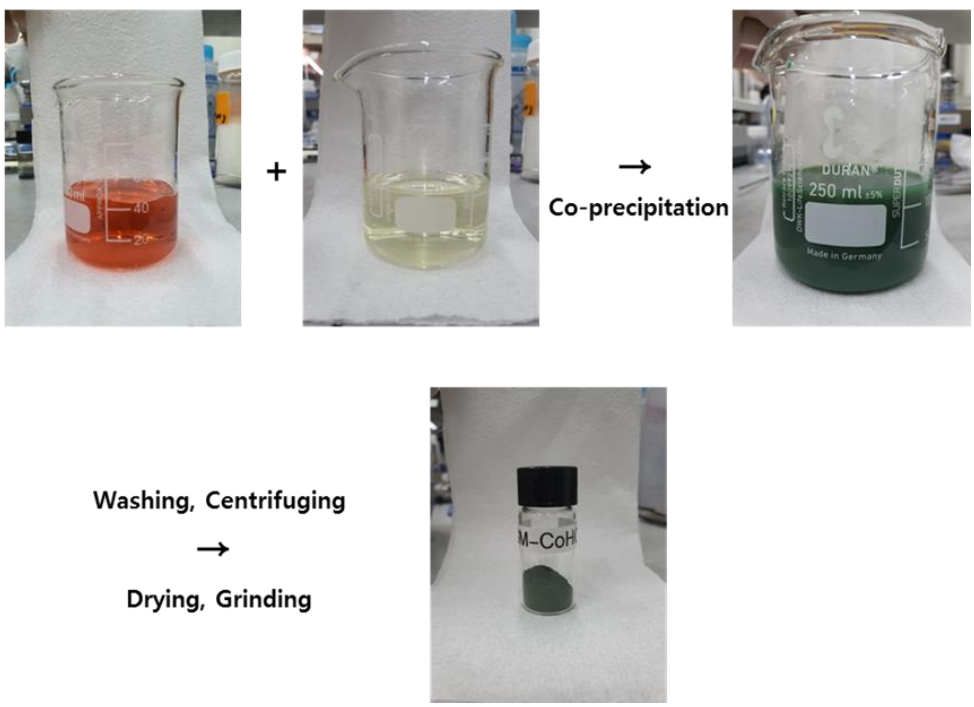


Figure 2. Photographic description of synthesis procedure of PBAs.

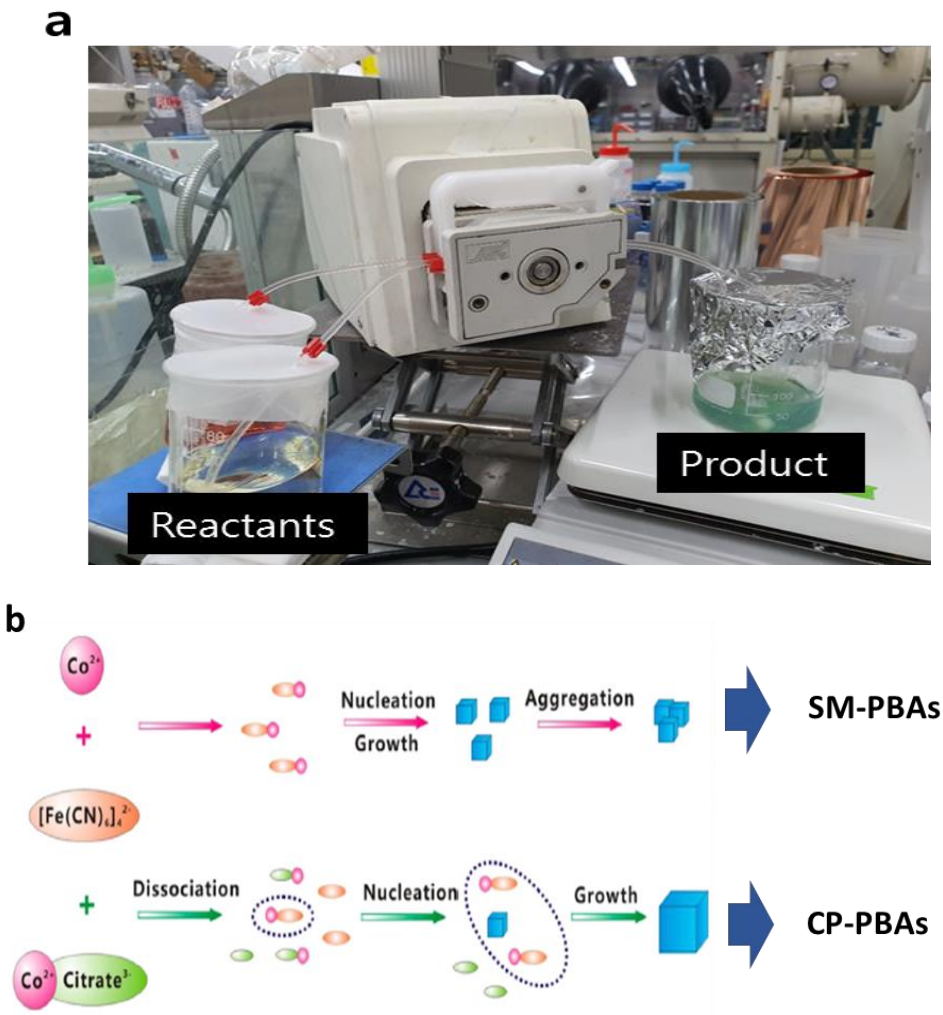


Figure 3. The synthesis of PBAs. (a)Photograph of co-precipitation synthesis of PBAs using peristaltic pump. (b) Schematic illustration of reaction process with and without chemical inhibition.

## 2.2 Charaterization

### *2.2.1 CoHCF*

As shown in SEM (Scanning Electron Microscope) images (Figure 4 a, b), CP-CoHCF has cubic-shaped morphology while SM-CoHCF has irregular morphology. X-ray diffraction (XRD) data presented in Figure 5, also show difference between CP-CoHCF and SM-CoHCF. Comparing two xrd data, peak intensity of CP-CoHCF is higher than SM-CoHCF which means CP-CoHCF has higher crystallinity. In addition, CP-CoHCF has a split peak at $2\theta$ ~24 ° Corres- ponding to (220) plane which does not appear in SM-CoHCF. This implies that two CoHCFs have different phase. It is known that when sodium ion's stoichiometric content is over the value of 1.5, rhombohedral phase rather than cubic appears [20]. The ideal chemical formula for synthesized CoHCF is $Na_{2-x}Co[Fe(CN)_6]_{1-y}*zH_2O$(x: 0~2, y: 0~1), where y is usually determined by the amount of $[Fe(CN)_6]^{2-}$ vacancy. To determine chemical formula of CP-CoHCF and SM-CoHCF, ICP-AES (Inductively Couple Plasma-Atomic Emission Spectrometer) analysis and TGA (Thermogravimetric Analysis) were conducted (Table 1, Figure 6 a). Here, x and y are determined by ICP-AES data which show the ratio of metallic elements, and z is determined by TGA data which show water content in gravimetric ratio. As a result, chemical formula for SM-CoHCF is determined as

$Na_{1.43}Co[Fe(CN)_6]_{0.85}$ $2.88H_2O$, and CP-CoHCF as $Na_{1.66}Co[Fe(CN)6]_{0.92}$ $1.8H_2O$. Through the different value of y (0.15 for SM-CoHCF and 0.08 for CP-CoHCF), it is concluded that slow reaction ensures low content of vacancy in crystal structure of CoHCF.

### *2.2.2 CuHCF*

SM-CuHCF and CP-CuHCF were synthesized in the same way as SM-CoHCF and CP-CoHCF were. As shown in SEM images (Figure 4 c, d), it can be confirmed that as the reaction rate becomes slow, the morphology of CuHCF becomes closer to the cube and the particle size of it also becomes larger. XRD data, also, show the same tendency with CoHCF in that CP-CuHCF has higher peak intensity, i.e. higher crystallinity than SM-CuHCF. However, split peak at $2\theta \sim 24^\circ$ cannot be found for CP-CuHCF, which means two CuHCFs have same phase (Figure 5 b). To determine chemical formula of SM-CuHCF and CP-CuHCF, ICP-AES analysis and TGA were carried out. As a result, the chemical formula of SM-CuHCF is $K_{0.09}Cu[Fe(CN)_6]_{0.7}$ $2.81H_2O$, and CP-CuHCF is $K_{0.05}Cu[Fe(CN)_6]_{0.68}$ $2.56\ H_2O$ (Table 2, Figure 6 b). Through the similar value of y (0.32 for SM-CuHCF and 0.3 for CP-CuHCF), it is concluded that slow reaction rate has no effect on repression of $Fe(CN)_6^{3-}$ vacancy formation. The precise cause of this phenomenon is not known. Recently, CuHCF with low vacancy (y=0.07) was reported, where ethanol is used instead of water and $[Fe(CN)_6]^{2-}$ ion instead of $[Fe(CN)_6]^{3-}$ from Yinzhu's group[21].

So, it can be assumed that the formation of vacancy is influenced by not only the rate of reaction but also the kinds of precursor used.

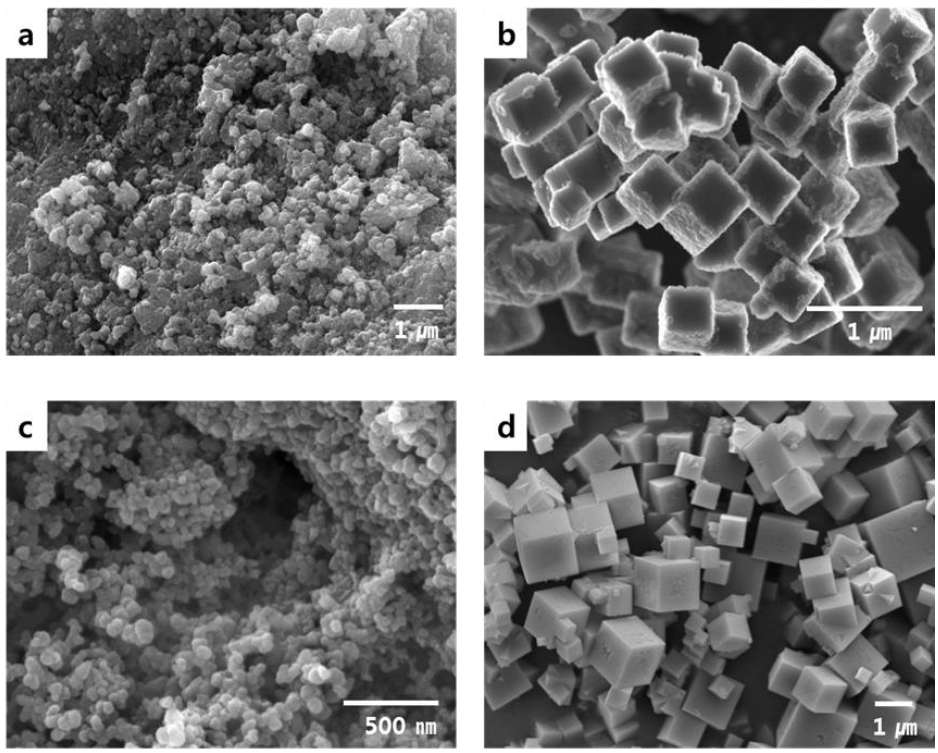


**Figure 4**. An SEM images of synthesized PBAs. (a)SM-CoHCF (b)CP-CoHCF (c)SM-CuHCF (d)CP-CuHCF

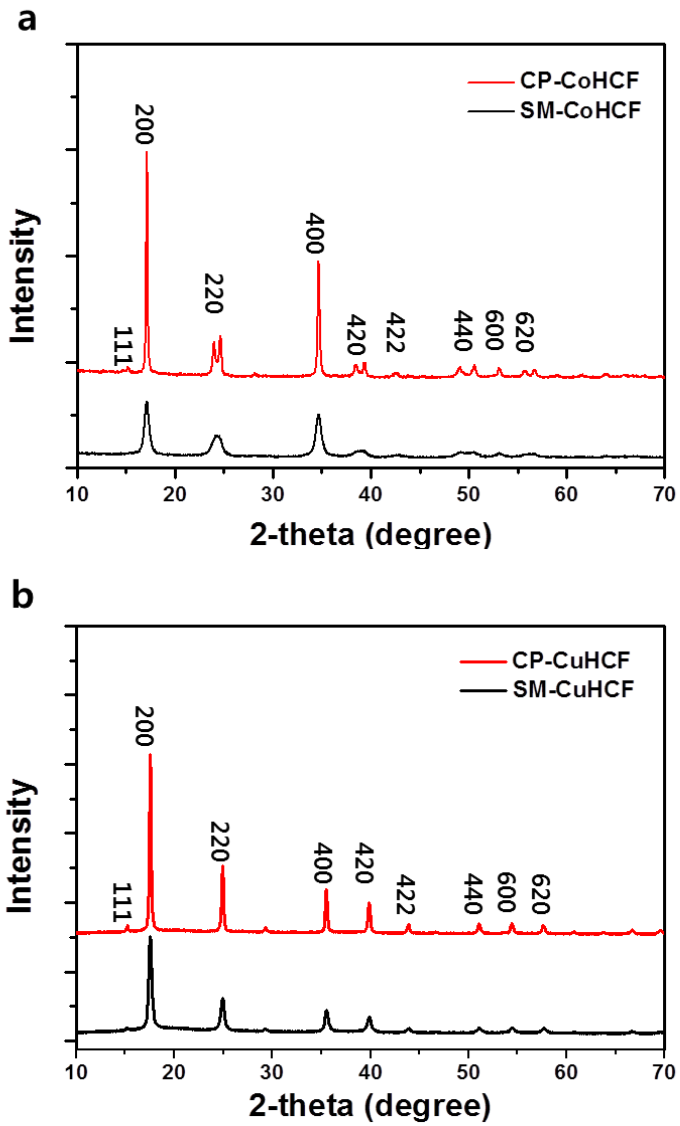


Figure 5. XRD patterns of synthesized PBAs. (a)CP-CoHCF and SM-CoHCF. (b) CP-CuHCF and SM-CuHCF.

| | Na | Co | Fe |
|---|---|---|---|
| CP-CoHCF | 46.3 | 27.93 | 25.77 |
| SM-CoHCF | 43.6 | 30.38 | 26.02 |

Table 1. Mole fraction (%) of metallic elements in CoHCFs.

| | K | Cu | Fe |
|---|---|---|---|
| CP-CuHCF | 5.26 | 55.58 | 39.16 |
| SM-CuHCF | 2.75 | 57.92 | 39.33 |

Table 2. Mole fraction (%) of metallic elements in CuHCFs.

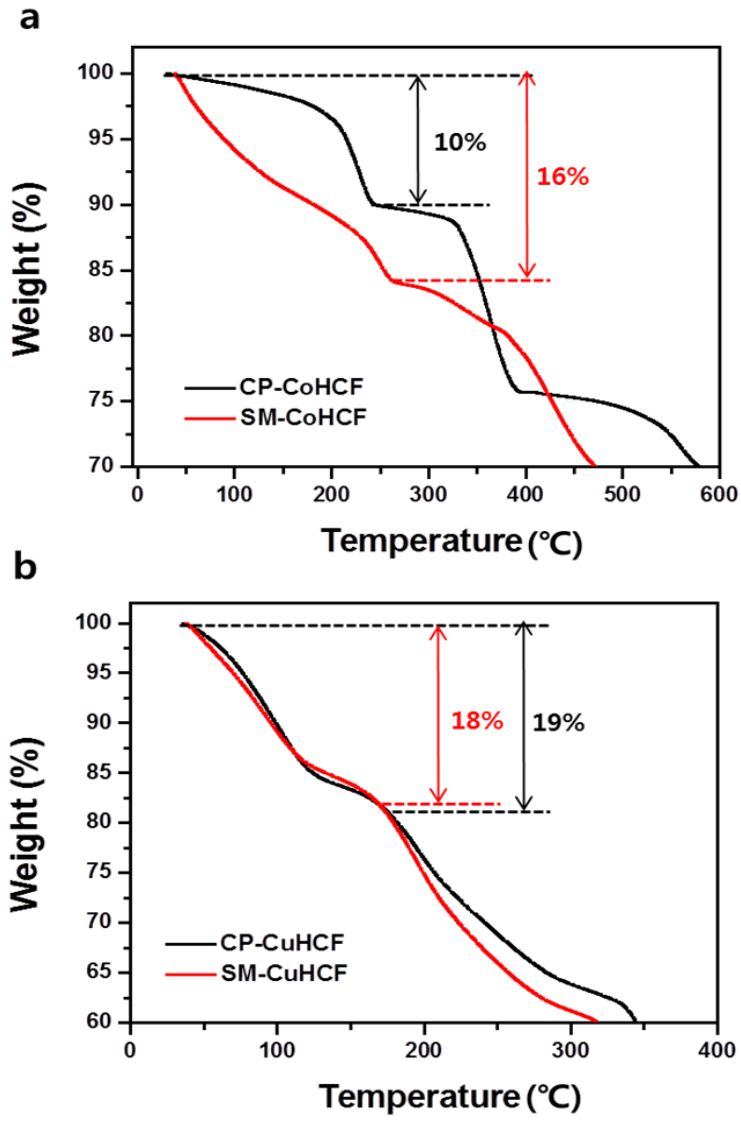


Figure 6. TGA data of PBAs. (a) CP-CoHCF and SM-CoHCF. (b) CP-CuHCF and SM-CuHCF.

## 2.3 Electrochemical performance

### *2.3.1 CoHCF for aqueous sodium ion battery cathode*

CoHCFs were electrochemically examined by preparing swagelok type three electrode cell in which activated carbon serves as counter electrode, Ag/AgCl electrode (0.21 V vs standard hydrogen electrode, S.H.E, hereafter all potential values are relative to Ag/AgCl electrode) as reference electrode and 1 m sodium ion aqueous solution as electrolyte. Because there are only subtle differences between CP-CoHCF and SM-CoHCF in terms of electrochemical reaction mechanism, here, only the property of CP-CoHCF is depicted for reaction mechanism analysis.

According to galvanostatic charge discharge plot (GCD) in figure 7 a, CP-CoHCF has a specific capacity of 111 mAh/g at 0.5 C (1 C = 100 mA/g) and two distinct plateaus appear at 0.4 V and 0.9 V. This can be confirmed more clearly in the differential capacity plot (dQ/dV vs V), where two distinct sharp peaks appear at 0.4 V and 0.9 V (Figure 7 b), which means an electrochemical reaction mainly occurs at these two potential values. In order to investigate the reaction mechanism more precisely, XANES (X-ray Absorption Near Edge Structure) analysis was conducted by using x-ray source of synchrotron. Three samples of fully charged, half-discharged and fully discharged were prepared and XANES analysis was carried out for cobalt and iron (Figure 8 a, b). As a result, in

the case of cobalt ion, the oxidation number was already changed when it was charged up to 0.5 V, thereafter, even after being fully charged up to 1 V, there was no significant change in the oxidation number. On the other hand, in the case of iron ion, the change of oxidation state only occurred when it was fully charged up to 1 V. These results can be translated that the electrochemical reaction occurs mainly due to redox reaction of cobalt ion at 0.4 V, and redox reaction of iron is responsible for electrochemical reaction at 0.9 V. So, the electrochemical reaction can be expressed by the following equation. (1 represents the reaction occurring at 0.2 V to 0.5 V and 2 at 0.5 V to 1 V)

$$Na_2Co(\text{II})Fe(\text{II})(CN)_6 \leftrightarrow NaCo(\text{III})Fe(\text{II})(CN)_6 + Na^+ + e^- \quad (1)$$

$$NaCo(\text{III})Fe(\text{II})(CN)_6 \leftrightarrow Co(\text{III})Fe(\text{III})(CN)_6 + Na^+ + e^- \quad (2)$$

Ex-situ XRD analysis was performed to look for changes in the structure of the CoHCF during the electrochemical reaction. As a result, there is a difference in peak shape at $2\theta \sim 24^\circ$ between charged state and discharged state (Figure 9). As mentioned above, different peak shape indicates different phase, so we can conclude that there is a phase transformation during electrochemical reaction of CoHCF in aqueous sodium ion battery system.

In order to figure out the difference of electrochemical performances according to the synthesis methods and crystallinity, electrochemical tests were performed on CP-CoHCF and SM-

CoHCF under same conditions. As you can see in Figure 10 a, which shows the change of capacity according to a rate of charge and discharge, CP-CoHCF shows higher capacity than SM-CoHCF in all C-rates, but their rate capabilities are similar. The higher capacity of CP-CoHCF is due to less formation of vacancies in the lattice, which means less loss of electrochemically active species (i.e. Fe), and the similarity of rate capability means that the resistance of charge transfer reaction and diffusion within CoHCF lattice for sodium ion is not greatly affected by crystallinity of CoHCFs. Meanwhile, to compare cyclability, CoHCFs were charged and discharged under 5 C-rate condition (Figure 10 b). It is revealed that the capacity retention of CP-CoHCF is much higher than SM-CoHCF. Through this data, higher durability of thermodynamically stable phase helps CoHCF endure the volume change accompanying with intercalation and deintercalation of carrier ion (i.e. sodium ion) during electrochemical reaction.

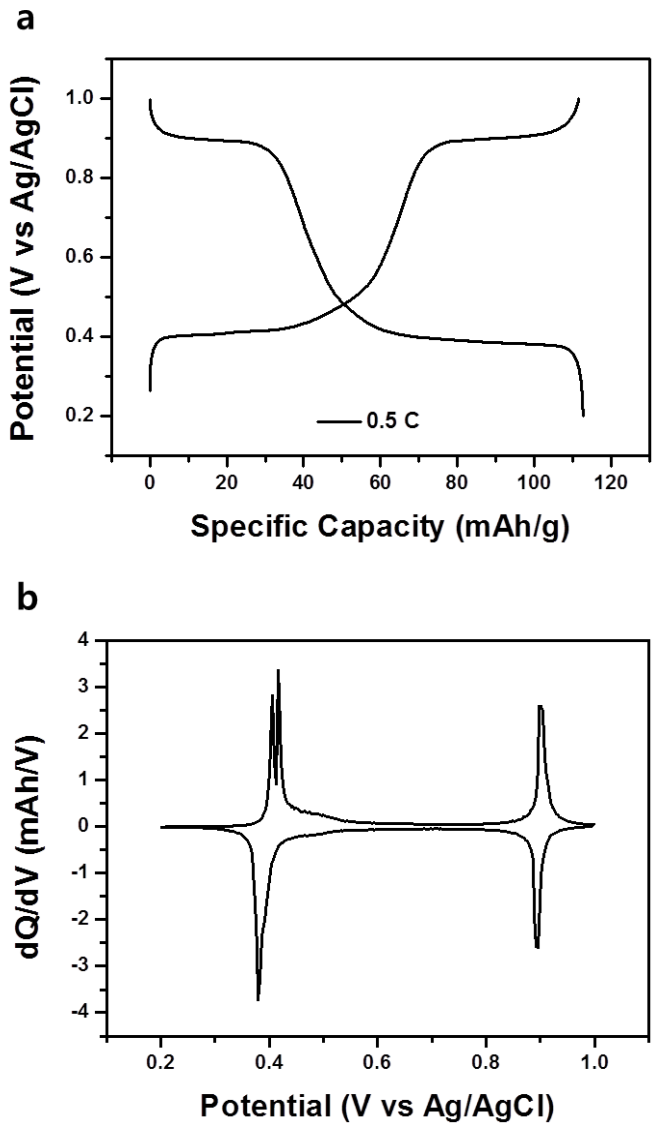


Figure 7. (a) Galvanostatic Charge Discharge plot of CoHCF in the range of 0.2 V – 1 V. (b) Differential capacity plot of CoHCF. The calculation for result of (b) is based on data of (a).

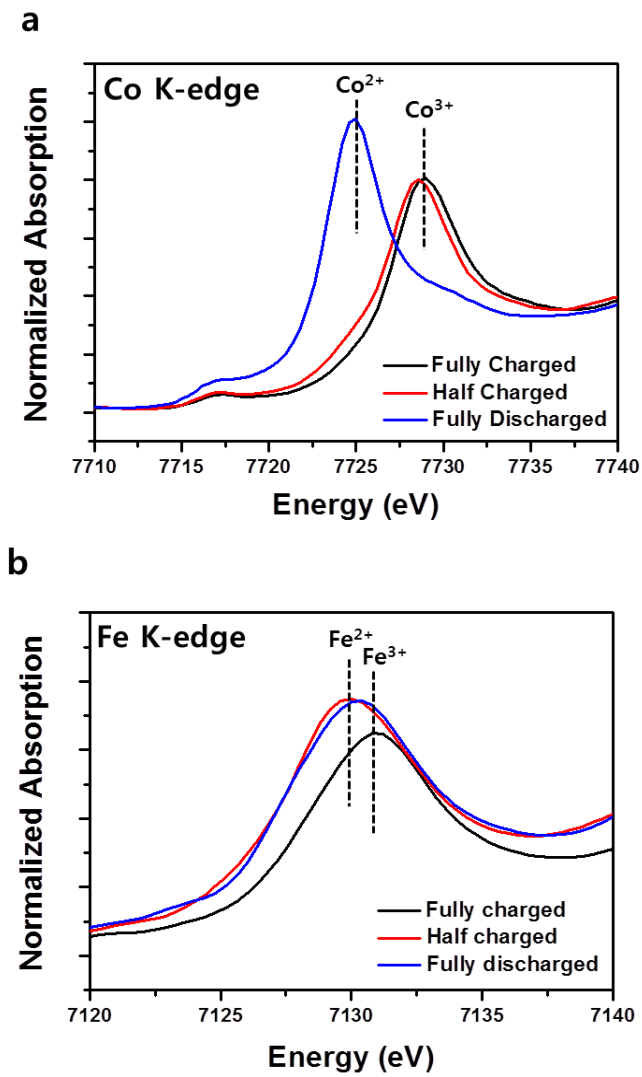


Figure 8. XANES plot of CoHCF electrode. (a) Cobalt K-edge peak. (b) Iron K-edge peak. The position of peak changes along with oxidation state. (Higher energy is corresponding to higher oxidation state)

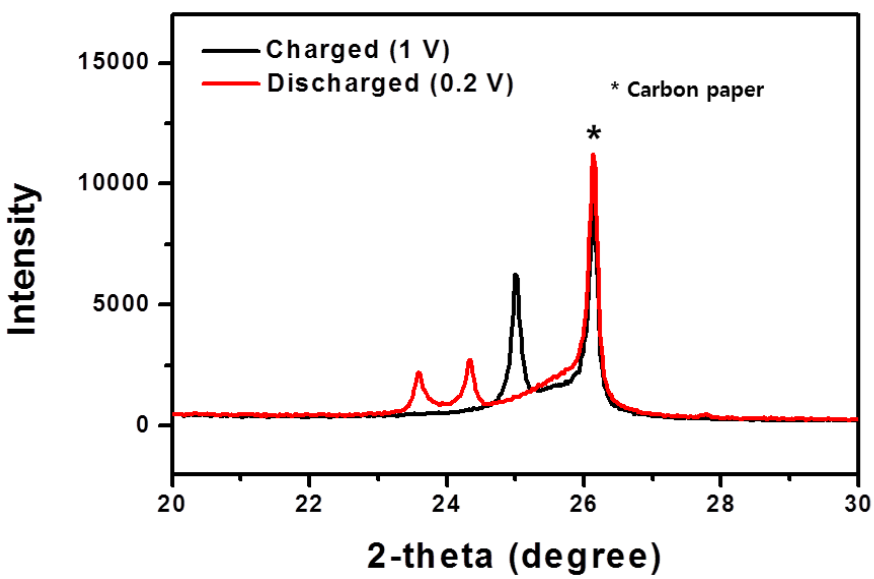


Figure 9. Ex-situ XRD plot of CoHCF electrode. During discharge, the peak moves to the left and splits. It means that upon insertion of sodium ion, volume of CoHCF expands and phase transformation occurs from cubic phase to rhombohedral phase. (The peak under asterisk belongs to current collector.)

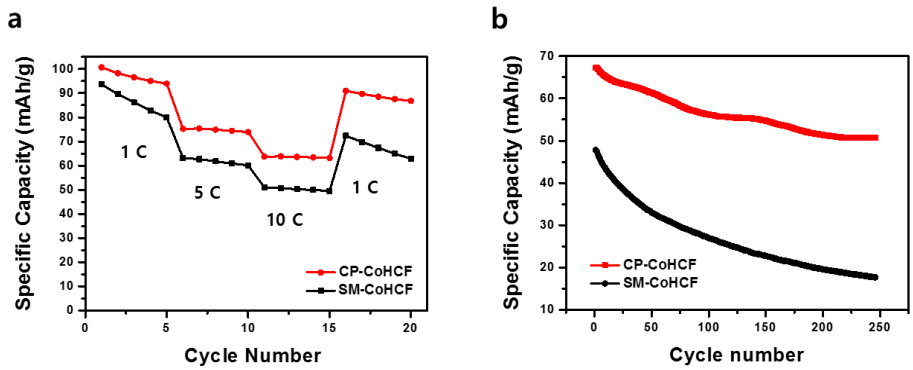


**Figure 10.** Comparison of electrochemical performance between CP-CoHCF and SM-CoHCF. (a) Rate capability profile. Compared to the specific capacity at 1C, that of 5 C was 80% and 10C was 68% for CP-CoHCF, and SM-CoHCF showed 79% and 63%, respectively. (b) Long-term cycle stability profile. CP-CoHCF showed 76% capacity retention over 250 cycles at 5 C, while SM-CoHCF show ed only 37%.

*2.3.2 CuHCF for aqueous zinc ion battery cathode*

CuHCF was electrochemically examined by preparing swagelok type three electrode cell in which zinc metal foil serves as counter electrode, Ag/AgCl electrode as reference electrode and zinc ion aqueous solution as electrolyte. As shown in Figure 11 a, CuHCF shows the capacity of 52 mAh/g at 1 C-rate (=50 mA/g) charge and discharge, and its differential capacity analysis shows two consecutive broad peaks at 0.6 V and 0.8 V (Inserted plot of Figure 11 a) where redox reaction mainly occurs. Meanwhile, pH value of aqueous zinc ion solution is smaller than 7 because zinc ion acts as Lewis acid and causes hydrolysis. So, proton ($H^+$) and zinc ion ($Zn^{2+}$) coexist in aqueous zinc ion solution and both of them are able to participate in electrochemical reaction. To determine which ion dominates the electrochemical reaction of CuHCF in zinc ion aqueous solution, two electrolytes with the same zinc ion concentration and different hydrogen ion concentrations were prepared. GCD tests were conducted both in electrolyte of pH 1 and pH 6, and compare the differential capacity analysis plot of them (Figure 11 b). Although the concentration of hydrogen ions differed by $10^5$ times, the peak positions were almost identical. So, it can be said that electrochemical reaction of CuHCF in zinc ion aqueous solution is dominated mainly by zinc ion.

To confirm the difference of electrochemical perform-ances according to synthesis method and crystallinity of CuHCF, electrochemical tests were performed on CP-CuHCF and SM-

CuHCF under same conditions. As a result, SM-CuHCF showed higher specific capacity at all C-rates, and also showed higher rate capability than CP-CuHCF (Figure 12). Surprisingly, these results are totally opposite to the electrochemical behavior of CoHCF for aqueous sodium ion battery where crystalline CoHCF showed higher specific capacity and both of CoHCFs had almost same rate capability. In order to translate this phenomenon, I compare the electrochemical behavior of sodium ion and zinc ion for SM-CuHCF to see the effect of intercalant. Electrochemical tests of CuHCF for sodium ion battery were executed with aqueous sodium ion solution under the same conditions as zinc ion battery. As shown in Figure 13 a, CuHCF showed the specific capacity of 58 mAh/g for sodium ion at 1 C-rate, and differential capacity analysis plot represented single peak around 0.7 V (Inserted in Figure 13 a). This is different from the result of zinc ion battery with two peaks, suggesting a different electrochemical behavior of the two systems. In addition, in the case of sodium ion, the specific capacity remained almost unchanged with changes in C-rate (Figure 13 b). (The reason why the capacity at 5 C is somewhat higher than the capacity at 1 C is that in case of an aqueous battery system, although high C-rate induces high over potential, it also suppresses the side reaction by water molecule) To investigate the reason for this difference of two ions, I compared electrochemical reaction mechanism of two different systems through ex-situ XANES analysis and ex-situ xrd analysis. For sodium ion battery system, the position of K-edge peak of copper ion did not change during charge/discharge process

and only iron ion was found to participate in the electrochemical reaction (Figure 14 a, b). For zinc ion battery system, I though the copper ion might show change in oxidation state because double peak was shown in differential capacity analysis plot. However, contrary to expectation, copper ion did not react in zinc ion battery system, neither (Figure 14 c, d) and the fact that only iron ion participate in electrochemical reaction can explain the reason why the specific capacity of CuHCF is only half that of CoHCF. Here, it is concluded that electrochemical reaction of CuHCF for sodium ion battery system and zinc ion battery system can be expressed by equation (3) and equation (4).

$$KCuFe(\text{Ⅲ})(CN)_6 + Na^+ + e^- \leftrightarrow NaKCu[Fe(\text{Ⅱ})(CN)_6] \quad (3)$$

$$KCuFe(\text{Ⅲ})(CN)_6 + \tfrac{1}{2}Zn^{2+} + e^- \leftrightarrow Zn_{0.5}KCu[Fe(\text{Ⅱ})(CN)_6] \quad (4)$$

Not only from the result of XANES analysis, but also with the ex-situ xrd data, noticeable difference between two systems could not be found (Figure 15 a, b). The sole difference is that zinc ion induced slightly larger lattice parameter change on CuHCF than sodium ion did. Therefore, in terms of electrochemical reaction mechanism, the difference between two systems could not be explained. So next, I approached in the aspect of kinetics.

To compare two systems from a kinetics point of view, EIS (Electrochemical Impedance Spectroscopy) analysis and CV (Cyclic Voltammetry) tests were performed. Nyquist plot of two systems is

shown in Figure 16, and it shows that there is greater resistance on the CuHCF when zinc ions participate in the electrochemical reaction, which is a series of process consists of charge transfer, solid state diffusion and bulk electrolyte diffusion. More detailed information about kinetics can be obtained through CV test. Generally, for CV test, the relationship between scan rate (v) and peak current ($I_p$) follows the equation 5.

$$I_p = av^b \quad (5)$$

$$\log(I_p) = \log(a) + b\log(v) \quad (6)$$

Constant b in equation 5 has a value between 0.5 and 1. It is known that when the value of b is close to 1, the system shows capacitive behavior with capacitor-like kinetics, and when it's value becomes close to 0.5, electrochemical reaction of the system is controlled by semi-infinite diffusion[22]. Equation 6 can be derived by taking log on both sides of equation 5 and the value of b corresponds to the slope of this equation. CV test was performed at a scan rate corresponding to the range from 1 mV/s to 100 mV/s for both of the systems (Figure 17 a, b). The results are depicted in Figure 17 c, and through linear fitting, the value of b for each system was obtained as 0.69 for sodium ion battery system and 0.83 for zinc ion battery system. This confirms that the electrochemical reaction of the zinc ion has more capacitive-like kinetics than sodium ion. Combined with the result of EIS analysis, it can be concluded that

the zinc ion has more difficulty in solid state diffusion within the lattice of CuHCF than the sodium ion. In view of this tendency, the two peaks that appeared in the differential capacity analysis plot of zinc ion battery system is due to the increase of overpotential arises from a repulsion force induced by early intercalated zinc ions.

Let's go back to the trend of rate capability of CuHCFs in aqueous zinc ion electrolyte. Putting the results of previous experiments together, unlike sodium ion, electrochemical performances of zinc ion depend on the length of diffusion path within the lattice of the CuHCFs. Therefore, for zinc ion, the shorter the diffusion path, the better the electrochemical performance. Meanwhile, as we confirmed earlier, particle size of CP-CuHCF is much larger than SM-CuHCF, resulting in longer diffusion path. This is because slow reaction induces small amount of nuclei formation in initial stage of the synthesis so that many of the reactants participate in growth of the particle. So, the trend that SM-CuHCF shows higher specific capacity and rate capability than crystalline CP-CuHCF is because SM-CuHCF has shorter diffusion path than CP-CuHCF.

Finally, long term cycle stability test was conducted (Figure 18 a). It was impossible to compare the degree of capacity retention between CP-CuHCF and SM-CuHCF, because the specific capacity of CP-CuHCF increased with the cycle. The cause of this phenomenon is not known precisely, but It is speculated that there is a transformation within the lattice of CuHCF during long term cycling in zinc ion electrolyte. To support this guess, cycle

stability test for SM-CuHCF was prolonged (Figure 18 b). As a result, the trend of capacity change after $100^{th}$ cycle is different from that of before $100^{th}$ cycle in that no reduction in capacity can be found. This trend can be confirmed more precisely by comparing differential capacity analysis plot of $50^{th}$ cycle with that of $150^{th}$ cycle (Figure 18 c, d). It is also supported by the report from Fabio's group where they insist that CuHCF separates into original CuHCF phase and new phase of ZnHCF after long term cycling [23].

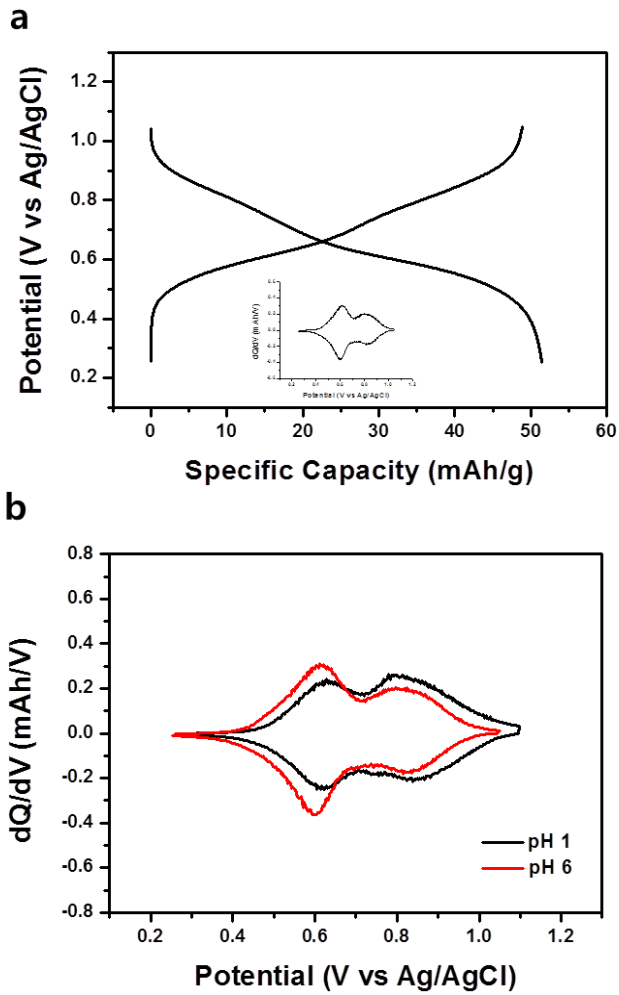


**Figure 11.** (a) GCD plot of CuHCF in aqueous zinc ion electrolyte at 1 C-rate(=50 mA/g) in the range of 0.25 V – 1.1 V. (b) Differential capacity analysis profile of CuHCF in aque-ous zinc ion electrolyte with different concentration of proton.

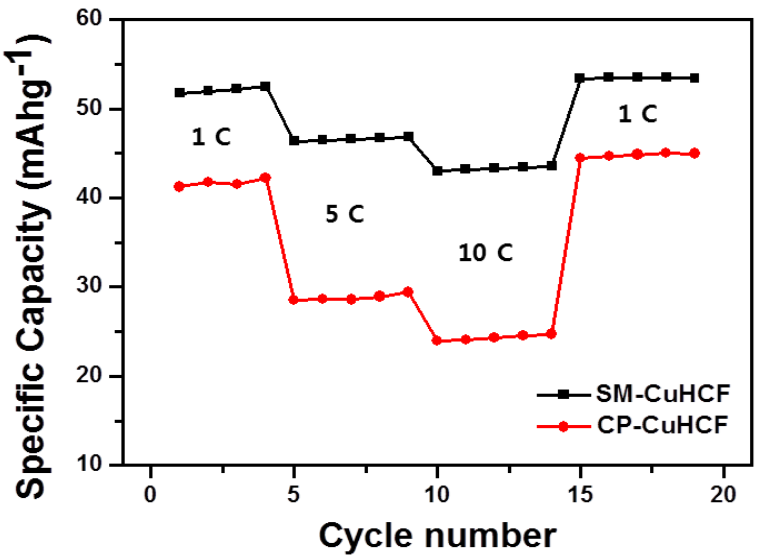


Figure 12. Rate capability profile of SM-CuHCF and CP-CuHCF. Compared to the specific capacity at 1 C, that of 5 C was 88% and 10 C was 82% for SM-CuHCF and CP-CuHCF showed 67% and 56% respectively.

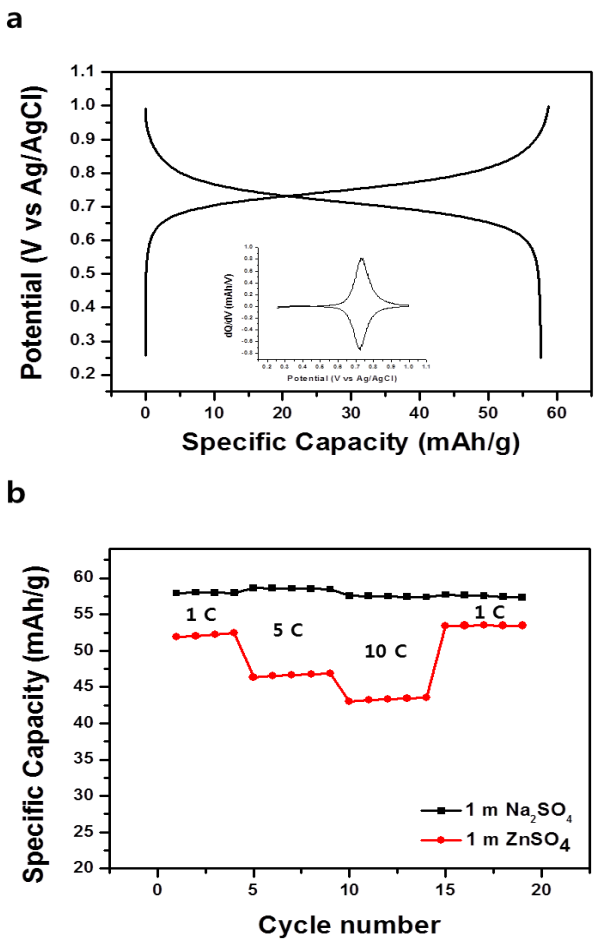


Figure 13. (a) GCD profile of CuHCF in sodium ion aqueous electrolyte at 1 C-rate (=50 mA/g) in the range of 0.25 V – 1 V. (b) Rate capability profile of SM-CuHCF in sodium ion and zinc ion aqueous solution. In sodium ion battery system, compared to the specific capacity at 1 C, that of 5 C was 101% and 10 C was 99%.

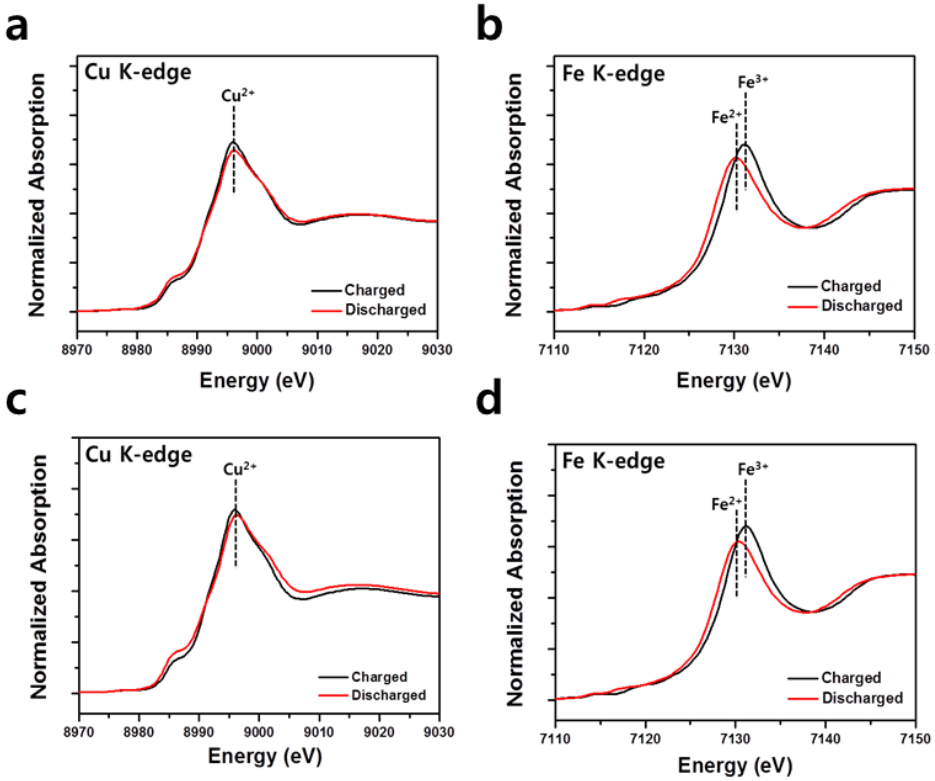


Figure 14. XANES plot of CuHCF electrode(a) Copper K-edge peak for sodium ion battery system. (b) Iron K-edge peak for sodium ion battery system. (c) Copper K-edge peak for zinc ion battery system. (d) Iron K-edge peak for zinc ion battery system.

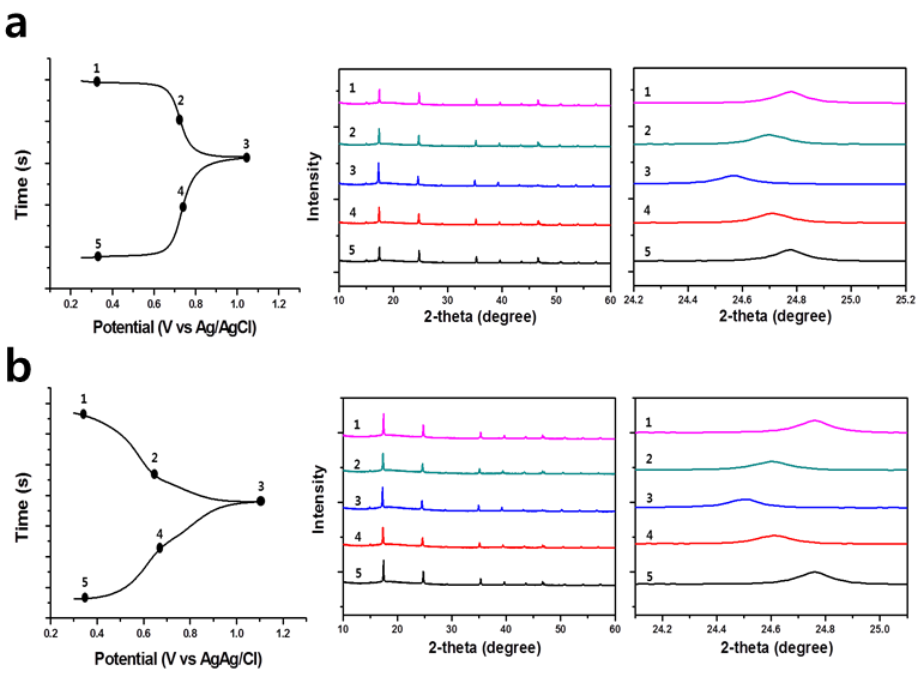


Figure 15. Ex-situ XRD patterns of CuHCF electrode at different state. (a)Sodium ion battery system. (b)Zinc ion battery system. Only a peak position shift exists without peak split.

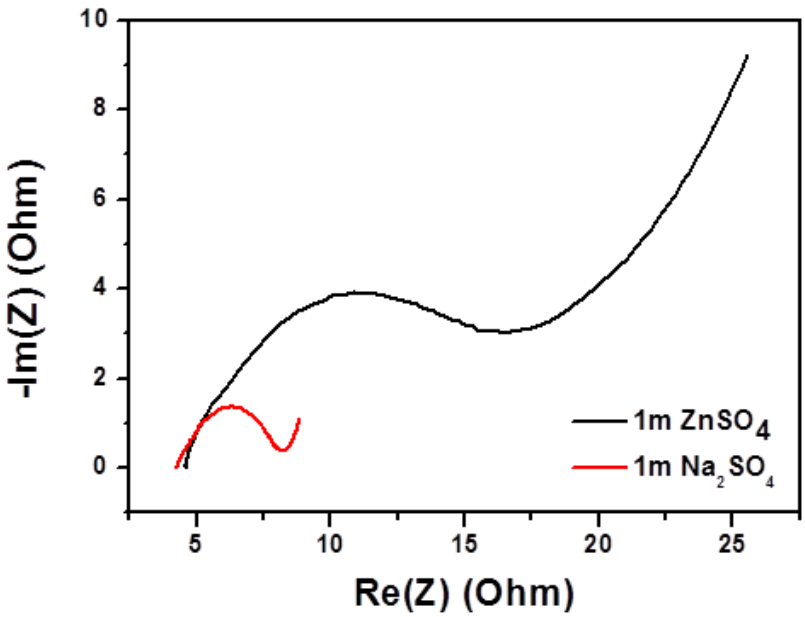


Figure 16. Nyquist plot of CuHCF in different electrolyte.

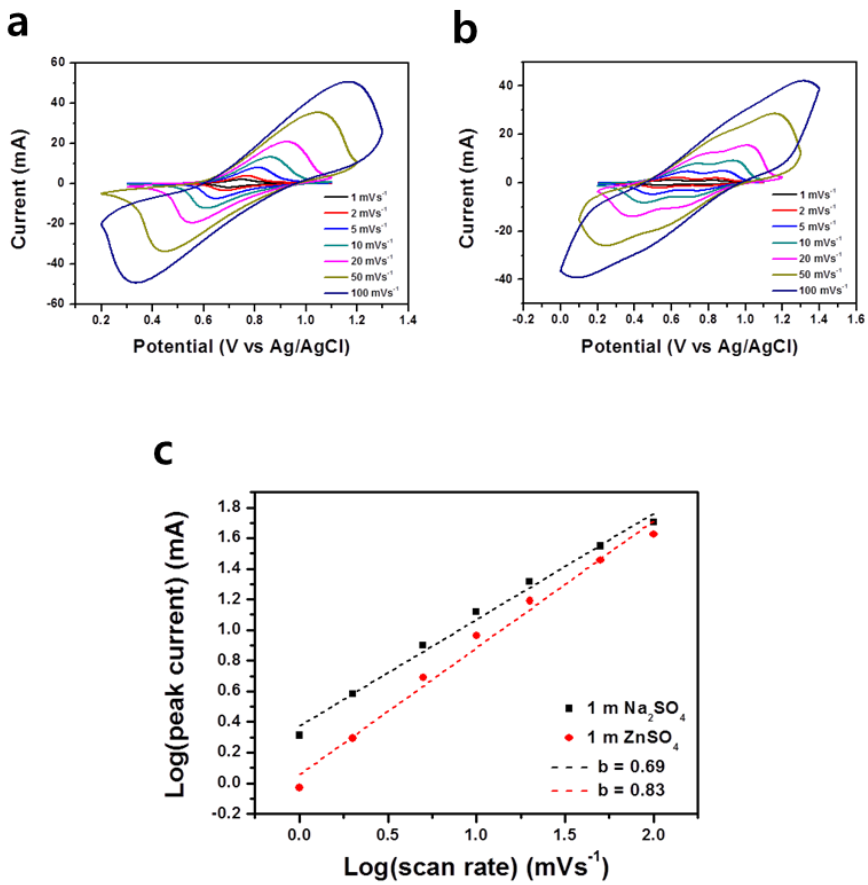


Figure 17. Cyclic voltammetry (CV) test of CuHCF in different electrolyte. (a)CV curves for sodium ion battery system at various scan rate. (b) CV curves for zinc ion battery system at various scan rate. (c) log($I_p$) versus log(v) plot for both of the electrochemical systems. Data of plot (C) are based on redox peak of CV curves in plot (a) and (b).

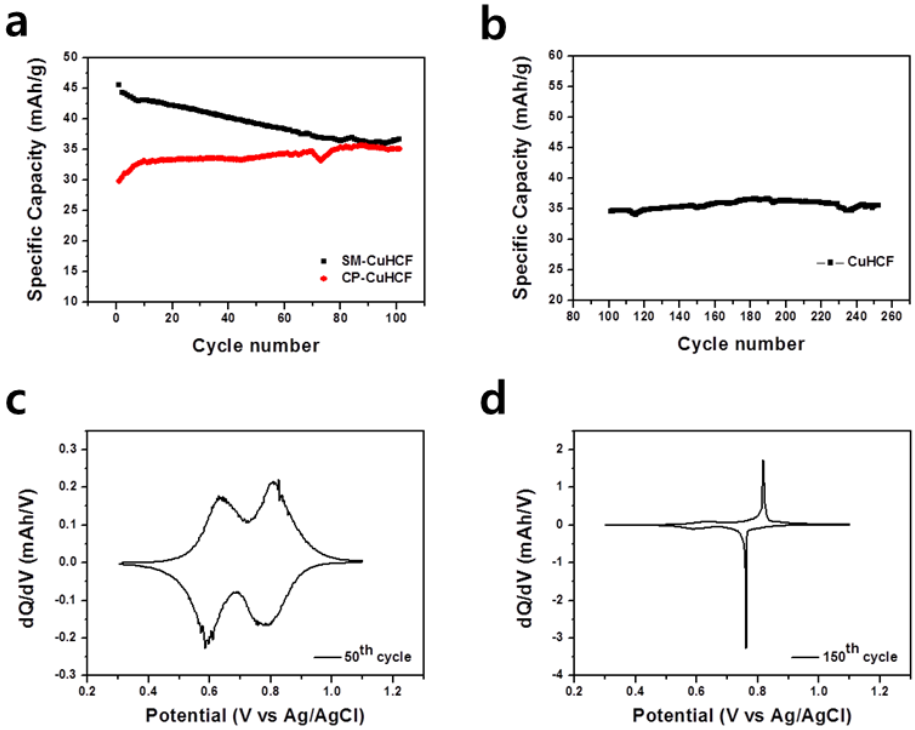


Figure 18. Long term cycle stability tests of CP-CuHCF and SM-CuHCF in aqueous zinc ion electrolyte at 5C (=250 mA/g). (a) Cycle performance of SM-CuHCF and CP-CuHCF up to 100$^{th}$ cycle. (b) Cycle performance of SM-CuHCF after 100$^{th}$ cycle. (c) Differential capacity analysis profile of 50$^{th}$ cycle. (d) Differential capacity analysis profile of 150$^{th}$ cycle.

# Chapter 3. Materials and Methods

## 3.1 Material synthesis

Copper(Ⅱ) nitrate hemi(pentahydrate), Cobalt(Ⅱ) nitrate hexahydrate, Sodium ferrocyanide(Ⅱ) decahydrate, potassium hexacyanoferrate(Ⅲ), sodium citrate tribasic dihydrate were purchased from Sigma Aldrich and all chemicals were used without further purification.

CP-CoHCF(CP-CuHCF) - First, equimolar amount of cobalt nitrate hexahydrate and sodium citrate tribasic di-hydrated were mixed in 50ml di water for 5 minutes to make 0.1 M solution. and then this solution and 0.1 M Sodium ferrocyanide decahydrate aqueous solution (50ml) were simultaneously added dropwisely to DI water (25 ml) by aid of peristaltic pump with constant stirring. The reaction temperature was maintained at 70℃ by hot plate. A green suspension was formed, and it was allowed to sit overnight. The precipitate was centrifuged to separate from water, washed with DI water and ethanol for 3 times to get rid of residual chemicals and dried in vacuum oven at 70℃ overnight. After that, it was grinded by using mortar to become a fine powder form. CP-CuHCF was synthesized in the same way except that copper nitrate hemi(pentahydrate) and potassium hexacyanoferrate were used and instead of green, brown precipitate was formed.

SM-CoHCF(SM-CuHCF) - 0.1 M cobalt nitrate hexahydrate aqueous solution (50ml) and 0.1 M Sodium ferrocyanide deca-hydrate aqueous solution (50ml) were added to DI water (25 ml) at once without peristaltic pump. After that, the rest of the process is same as CP-CoHCF. SM-CuHCF was synthesized in the same way with copper nitrate hemi (pentahydrate) and potassium hexacyano-ferrate.

## 3.2 Characterization

The morphologies of synthesized PBAs were characterized by field-emission scanning electron microscopy (FE-SEM, JEOL, JSM-7800F Prime). And the chemical composition of PBAs was determined by Inductively Coupled Plasma-Atomic Emission Spectroscopy (ICP-AES, Perkin-Elmer, OPTIMA 8300) and the water content was obtained by Thermal Gravimetry Analysis (TGA, TA Instruments, Discovery TGA). The crystal structure of PBAs was characterized by Powder X-ray diffraction (PXRD, Rigaku, SmartLab) at the scan rate of 2 degree per minute in the range of 10 degree to 70 degree. Crystal structure transformation during electrochemical reaction was investigated by ex-situ X-ray diffraction method using 9B Beamline of Pohang Accelerator Laboratory (PAL). To investigate electrochemical reaction mechanism of PBAs, ex-situ X-ray Absorption Near Edge Spectroscopy (XANES) was performed through 7D Beamline of

PAL. For 'ex-situ' experiments, electrode samples were electrochemically tested in the form of beaker type three electrode cell and allowed to rest at specific potential for several hours until equilibrium was reached. After that, they were taken out from the beaker cell, washed with DI water several times, and vacuum dried at room temperature.

## 3.3 Electrochemical Characterization

Sodium sulfate, zinc sulfate heptahydrate were purchased from Sigma Aldrich and used without further purification.

### *3.3.1 Cell Fabrication*

The synthesized PBAs were first mixed with Super P (conductive material) and Polyvinylidene fluoride (PVdF, binder) in weight ratio of 7:2:1 (Active material : conductive material : binder) and 1-methyl-2-pyrrolidone (NMP) was added to form homogeneous slurries. The slurry was cast onto carbon current collector (280㎛ thick carbon paper, TGP-H-090, Toray) and dried in the vacuum oven overnight. The mass loading of active material was 2~4 mg/cm2. Activated Carbon electrode was prepared in the same way as PBAs electrode except that activated carbon (YP-50F) and PVdF were mixed in weight ratio of 9:1.

Swagelok type cell consist of Teflon body and SUS bar. For swagelok type cell preparation, the PBAs electrodes were punched into 10 pi circular discs, and counter electrodes (250㎛ thick zinc metal foil, Alfa aesar and activated carbon electrode) were punched into 12 pi circular discs. The swagelok-type cell was assembled by sandwiching separator (GF/D filter paper, Whatman) between PBAs electrode and counter electrode. Ag/AgCl reference electrode (RE-1B, Qurins) was also placed together like figure 19 a. For beaker cell preparation, PBAs electrodes were fabricated as bar-type electrode, where electrode slurries were cast on rectangular form carbon paper (15mm×60mm) with 10 pi circular shape (Figure 19 b). 1m Zinc sulfate and 1m sodium sulfate were used as electrolyte and purged with nitrogen gas for 30minutes before using to eliminate dissolved oxygen [24].

### *3.3.2 Electrochemical Test*

Electrochemical tests were carried out by potentiostat (SP-50 and SP-150, BioLogic). Before cycling test and Galvanostatic charge/discharge (GCD) test, all of the samples had pre-cycle operating at 0.5 C (50mA/g for CoHCF, 25 mA/g for CuHCF). Electrochemical Impedance Spectroscopy (EIS) for CuHCF was performed in the range from $10^{-1}$ to $10^{6}$ Hz at the half charged(discharged) state and differential capacity analysis is conducted using battery analysis function of EC-Lab potentiostat program.

a

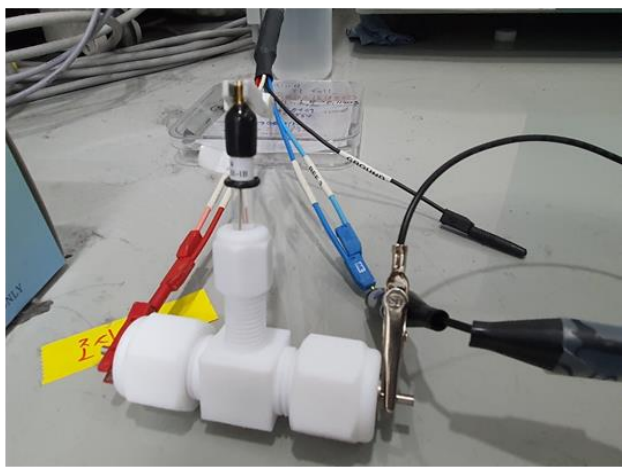

b

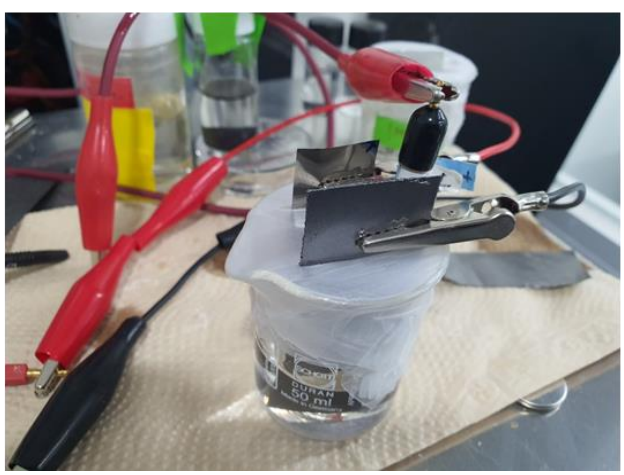

**Figure 19.** Photograph of electrochemical cell configuration. (a) Swagelok type three electrode cell. (b) Beaker type three electrode cell.

# Chapter 4. Conclusion

To investigate correlation between synthesis method of PBAs and its electrochemical performance, thermodynamically stable form of PBAs (CP-CoHCF and CP-CuHCF) and their counterparts with thermodynamically unstable form (SM-CoHCF and SM-CuHCF.) were synthesized by controlling the rate of synthesis. For CoHCF as aqueous sodium ion battery cathode, slowly synthesized CP-CoHCF has low vacancy and high crystallinity, which make it have higher specific capacity and cycle stability. However, for CuHCF, slow synthesis did not guarantee low vacancy. Also, as a cathode material of a zinc ion battery, CuHCF shows different tendency from CoHCF in that rapidly synthesized SM-CuHCF has higher specific capacity and rate capability than slowly synthesized CP-CuHCF. Performing several electrochemical tests with CuHCF in different electrolyte, it was concluded that the species of carrier cation, i.e. charge density of it, made the difference. This study gave us the insight that the design of the PBAs electrodes should be different depending on the target electrochemical system. In depth studies of the detailed ion diffusion, storage and phase transformation mechanism should be done to improve the electrochemical performance of PBAs.

# Bibliography


[1] B. Dunn, H. Kamath, J. –M. Tarascon, *Science*, 2011, 334, 928–935.

[2] Z. Yang, J. Zhang, M. C. W. Kintner–Meyer, X. Lu, D. Choi, J. P. Lemmon, J. Liu, *Chem. Rev.*, 2011, 111, 3577–3613.

[3] N. Alias, A. A. Mohamad, *J. Power Sources*, 2015, 274, 237–251.

[4] J. –M. Tarascon, *Nat. Chem.*, 2010, 2, 510.

[5] J. Qian, C. Wu, Y. Cao, Z. Ma, Y. Huang, X. Ai, H. Yang, *Adv. Energy. Mater.,* 2018, 1702619.

[6] S. –W. Kim, D. –H. Seo, X. Ma, G. Ceder, K. Kang, *Adv. Energy. Mater.*, 2012, 2, 710–721.

[7] J. C. Pramudita, D. Sehrawat, D. Goonetilleke, N. Sharma, *Adv. Energy. Mater.*, 2017, 7, 1602911.

[8] M. M. Huie, D. C. Bock, E. S. Takeuchi, A. C. Marschilok, K. J. Takeuchi, *Coordination Chemistry Reviews*, 2015, 287, 15–27.

[9] R. J. Gummow, G. Vamvounis, M. B. Kannan, Y. He, Adv. Mater., 2018, 30, 1801702

[10] J. Shin, D. S. Choi, H. J. Lee, Y. Jung, J. W. Choi, *Adv. Energy. Mater.*, 2019, 9, 1900083.

[11] D. J. Kim, D. –J. Yoo, M. T. Otley, A. Prokofjevs, C. Pezzato, M. Owczarek, S. J. Lee, J. W. Choi, J. F. Stoddart, *Nat. Energy*, 2018, 4, 51–59.

[12] G. L. Soloveichik, *Annu. Rev. Chem. Biomol. Eng.,* **2011**, 2, 503-527.

[13] S. P. Ong, V. L. Chevrier, G. Hautier, A. Jain, C. Moore, S. Kim, X. Ma, G. Ceder*, Energy Eviron. Sci.*, **2011**, 4, 3680.

[14] H. Kim, J. Hong, K. -Y. Park, H. S. Kim, S. -W. Kim, K. Kang, *Chem. Rev*. **2014**, 114, 11788-11827.

[15] F. Herren, P. Fischer, A. Ludi, W. Hälg, *Inorg. Chem.,* **1980**, 19, 956.

[16] H. W. Lee, R. Y. Wang, M. Pasta, S. Woo Lee, N. Liu, Y. Cui*, Nat. Commun.*, **2014**, 5, 5280.

[17] C. J. Xu, B. H. Li, H. D. Du, F. Y. Kang, *Angew. Chem. Int. Ed.*, **2012**, 51, 933.

[18] F. Scholz, A. Dostal, *Angew. Chem. Int. Ed.,* **1995***,* 34*,* 2685-2687.

[19] R. Chen, Y. Huang, M. Xie, Z. Wang, Y. Ye, L. Li, F. Wu, *ACS Appl. Mater. Interfaces*, **2016**, 46, 31669-31676.

[20] Y. Moritomo, K. Igarashi, T. Matsuda, J. Kim, *J. Phys. Soc. Jpn.*, 2009, 78, 074602.

[21] B. Wang, S. Liu, W. Sun, Y. Tang, H. Pan, M. Yan, Y. Jiang, *ChemSusChem*, **2019**, 12, 2415-2420.

[22] M. Toupin, T. Brousse, D. Belanger, *Chem. Mater.,* **2004**, 16, 3184-3190.

[23] G. Kasiri, R. Trocoli, A. B. Hashemi, F. L. Mantia, *Electrochimica Acta*, **2016**, 222, 74-83.

[24] J. -Y. Luo, W. -J. Cui, P. He, Y. -Y. Xia, *Nature Chem*, **2010**, 2, 760-765.

# 국문초록

프러시안블루 유사체 (Prussian blue analogues, PBAs)는 유무기 복합체의 일종으로 고유의 열린 골격구조 덕분에 수화된 이온의 삽입/탈리를 동반하는 수계배터리 시스템이나 리튬보다 큰 이온반경을 갖는 이온들을 이용한 배터리 시스템과 같은 차세대 배터리의 양극재로 주목을 받고 있다. 프러시안블루 유사체의 합성은 매우 간단하고 경제적인데 반해, 그 반응속도가 굉장히 빠르기 때문에 합성조건에 따라 다양한 구조적 성질을 갖는 반응물이 만들어진다. 서로 다른 합성환경에서 비롯된 결정구조의 차이가 전기화학적 성능에 미치는 영향을 알아보기 위해 아주 빠르거나 혹은 아주 느린 서로 다른 두 가지의 합성방법으로 프러시안블루 유사체를 합성하여 수계 소듐이온전지 시스템과 수계 아연이온전지 시스템에서 전기화학성능평가를 진행하였다. 그 결과, 수계 소듐이온전지 시스템에서는 느리게 합성된 프러시안블루 유사체가 빠르게 합성된 것보다 더 높은 전기화학성능을 나타낸 반면, 수계 아연이온전지 시스템에서는 반대의 경향이 나타났다. 이러한 경향 성의 원인을 조사하기 위해 더 다양한 전기화학실험을 활용하여 프러시안블루 유사체를 전극으로 사용한 수계 소듐이온전지 시스템과 수계 아연이온전지 시스템을 직접 비교하였고, 두 종류의 이온이 고체상 확산의 측면에서 서로 다른 전기화학거동을 보인다는 사실을 발견하였다. 이러한 일련의 결과들은 프러시안블루 유사체의 구조적 성질과 이에 따른 전기화학성능이 전기화학반응에 참여하는 이온의 종류에 따라 다르다는 사실을 말해주고 있다.